Modeling of three-phase continuously operating open-cell foam catalyst packings

Najarnezhadmashhadi, Ali; Braz, Catarina G.; Russo, Vincenzo; Eränen, Kari; Matos, Henrique A.; Salmi, Tapio

Published in:
AIChE Journal

DOI:
10.1002/aic.17732

Published: 01/09/2022

Document Version
Final published version

Document License
CC BY

Received: 7 December 2021 | Revised: 2 April 2022 | Accepted: 19 April 2022

DOI: 10.1002/aic.17732

RESEARCH ARTICLE

Reaction Engineering, Kinetics and Catalysis

AIChE JOURNAL

Modeling of three-phase continuously operating open-cell foam catalyst packings: Sugar hydrogenation to sugar alcohols

Ali Najarnezhadmashhadi[1] | Catarina G. Braz[2] | Vincenzo Russo[3] | Kari Eränen[1] | Henrique A. Matos[2] | Tapio Salmi[1]

[1]Laboratory of Industrial Chemistry and Reaction Engineering, Johan Gadolin Process Chemistry Centre (PCC), Åbo Akademi University, Turku/Åbo, Finland

[2]Centro de Recursos Naturais e Ambiente, Instituto Superior Técnico, Universidade de Lisboa, Lisbon, Portugal

[3]Chemical Sciences Department, Università di Napoli "Federico II," Complesso Universitario Monte S. Angelo, Naples

Correspondence
Vincenzo Russo, Chemical Sciences Department, Università di Napoli "Federico II," Complesso Universitario Monte S. Angelo, IT-80126 Naples, Italy
Email: v.russo@unina.it

Funding information
Academy of Finland, Grant/Award Number: 319002; Rector of Åbo Akademi University (Ali Najarnezhadmashhadi); Neste-Fortum Foundation; Finnish Cultural Foundation

Abstract

An advanced comprehensive and transient multiphase model for a trickle bed reactor with solid foam packings was developed. A new simulation model for isothermal three-phase (gas–liquid–solid) catalytic tubular reactor models was presented where axial, radial, and catalyst layer effects were included. The unique feature of this model is that the material balances include most of the individual terms (i.e., internal diffusion, gas–liquid, and liquid solid mass transfer, kinetics) for solid foam packing which is seldom done. Hydrogenation of arabinose and galactose mixture on a ruthenium catalyst supported by carbon-coated aluminum foams was applied as a fundamentally and industrially relevant case study. Parameter estimations allowed to obtain reliable and significant parameters. The effect of the kinetic parameters and the operation conditions on the arabinose and galactose conversions was studied in detail by sensitivity analysis. The model described is applicable for other three-phase continuous catalytic reactors with solid foam packings.

KEYWORDS
gPROMS, kinetics, mass transfer, open cell foam catalyst packing, structured catalyst, trickle bed reactor

1 | INTRODUCTION

Energy-efficient technologies have been an aspiration for the chemical industries, especially the design of chemical reactors. Structured catalysts play an important role to achieve this purpose. Several types of structured catalysts have been invented and investigated in recent years, such as monoliths, fibers, solid foams as well as structures prepared by three-dimensional (3D) printing. In a broad sense, many milli- and microreactors can be regarded as structured catalytic reactors. The characteristic feature for a structured chemical reactor is that the solid catalyst is kept immobile by fixing the catalyst carrier on the walls of the reactor channel (e.g., monolith and microreactor channels) or by installing the structured catalyst as an integrated part of the reactor tube.

For catalytic three-phase systems (solid catalyst, gas phase, and liquid phase) the even distribution of the gas and liquid phases is a challenge for classical structured catalysts, such as monoliths. The distribution problem can be solved with tailored structures in laboratory scale, but the process scale up is demanding, because reliable and inexpensive distribution systems are required. Therefore, the interest in randomly organized structured catalysts, such as solid foams is growing. Simply speaking, if the solid catalyst itself is random, there is a hope that it helps to randomize the gas and liquid flows through the reactor. Solid foams have been originally proposed for heat exchange,

but in the recent years the interest in solid foam scaffolds for heterogeneous catalysts has been growing all over the world.

Due to the fact that solid foam catalysts provide a high porosity (75%–95%) and a high specific surface area, open cell foam catalyst packings have recently been investigated as an alternative for catalytically active reactor packings. Enhanced mass and heat transfer, suppressed pressure drop and high specific surface area are important features of the solid foam packings.[1–9] Furthermore, the structures of pores and struts in open cell foams allow radial liquid flow and local turbulence which result in enhanced mass and heat transfer. In comparison with particle packings, solid foams have higher overall mass and heat transfer rates. Also, axial and radial mixing are improved by the high pore tortuosity of solid foams.[10,11] Thin catalyst layers (typically <<10 μm) used in solid foams improve the internal mass transfer in the catalyst pores, which leads to higher effectiveness factors compared with catalyst pellets with thicker catalyst layers (up to 1 cm). Based on the characteristic features mentioned, open cell foam catalysts are valuable as reactor packing materials and beneficial for continuous tubular reactors.

In this work, advanced multiphase modeling and simulation of the hydrogenation of arabinose and mixture of arabinose and galactose in a tubular reactor packed with open cell aluminum foam catalysts were developed. The catalyst was ruthenium on active carbon coating (Ru/C) on the surface of aluminum foam.[12] The system has been studied for reactor performance characterization and mass transfer measurements.[13–15] Tubular reactor with a diameter of 11 mm and bed length of 33 mm equipped with open cell aluminum foam was applied for the modeling (Figure 1). The foams had a pore density of 40 PPI. The experimental results have been discussed in a previous article published by our group.[8]

Three-phase catalytic tubular reactor models were developed for solid foam packings. The unique feature of this model is that the gas, liquid and solid phase mass balances include most of the individual terms such as internal diffusion, gas–liquid and liquid solid mass transfer and intrinsic kinetics. Furthermore, the gas and liquid flows are described by axial and radial dispersion terms along with liquid hold-up and pressure drop expressions. Previous studies and review articles have been published for this kind of modeling approach for a trickle bed reactor (TBR).[13,16] We have developed a fast running two-dimensional (2D) model and gPROMS software (Process System Enterprise) was used for the implementation. Compared with models based on computational fluid dynamics (CFD) which demands heavy computations for multiple parameter estimation purposes,[17–19] gPROMS provides fast computations and parameter estimation results at a reasonable time.

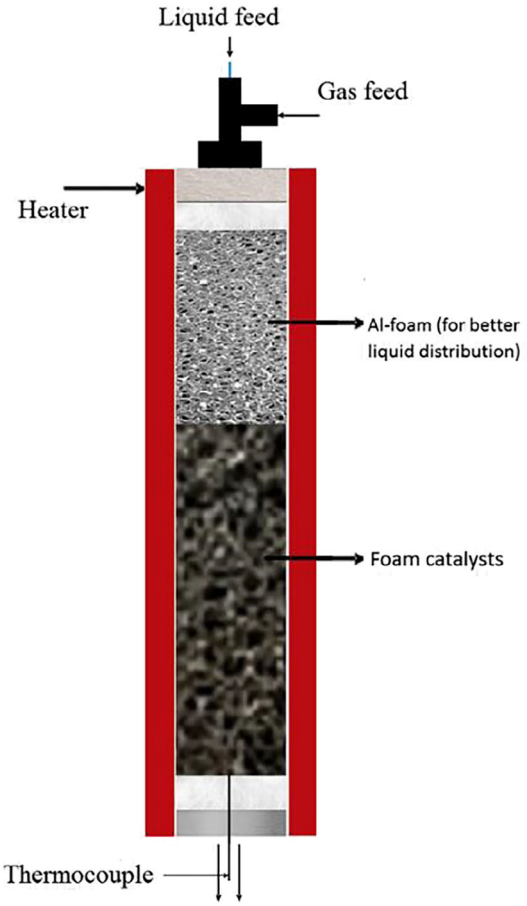

FIGURE 1 Continuous tubular reactor system: trickle bed with a cylindrical solid foam packing

2 | MODELING PRINCIPLES AND MODEL EQUATIONS

2.1 | Models for continuous trickle bed reactor with open cell foam packing

Besides the intrinsic kinetics and flow pattern, the heat and mass transfer effects are critical issues in the mathematical modeling of solid foam structures. Heat and mass transfer resistance can appear at the gas–liquid interface, at the liquid–solid interface as well as inside the pores of the catalyst layer. The transport resistances at the gas–liquid and liquid–solid interfaces depend strongly on the flow conditions, that is, on the Reynolds number. At low velocities the Reynolds number is low which implies that the Sherwood and Nusselt numbers are low and, consequently, the heat and mass transfer coefficients obtain low values. Many organic reactions applied in the production of fine and specialty chemicals and ingredients in alimentary products, are slow, which means that rather long residence times in the reactor are necessary to obtain a high conversion. Long residence times often imply low flow velocities in the reactor.

The impact of the internal mass transfer effects, on the other hand, depends on the ratio of the reaction and diffusion rates and the thickness of the catalyst layer. A common statement for catalytic processes carried out in structured reactors with thin catalyst layers (typically 50 μm or less) is that the internal mass transfer resistance in the catalyst pores is negligible. However, the role of internal mass transfer can become prominent even for thin catalyst layers if the chemical reaction is rapid and diffusion is slow. Therefore, two different versions of the mathematical model are treated in detail in this study: a

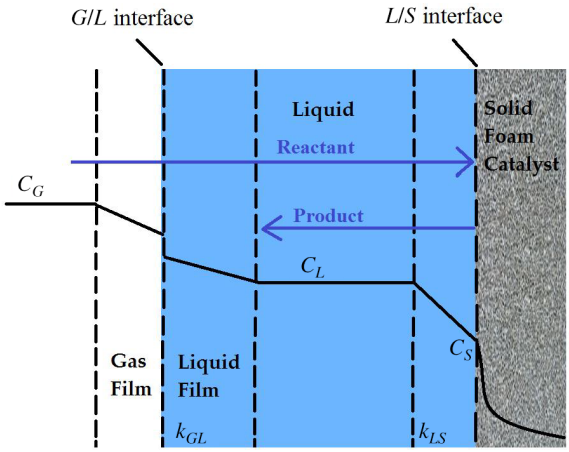

FIGURE 2 Interaction of kinetic and mass transfer effects in the tree-phase system: gas, liquid, and solid foam catalyst

simplified model, where the gas–liquid and liquid–solid mass transfer resistance is considered and an advanced model, which includes the internal mass transfer resistance, too. Catalytic hydrogenation of sugars to sugar alcohols is taken as the case study. Because the experiments were carried out with dilute solutions of the sugars and the reaction enthalpy of sugar hydrogenation is moderate (-82.0×10^3 J/mol),[13] the treatment is limited to isothermal cases. The system is schematically illustrated in Figure 2.

3 | SIMPLE MODEL

Time dependent concentrations at different locations (axial and radial position) inside the tubular reactor were acquired by solving mass balances, which include the kinetic rate laws, and fluid dynamic expressions. The set of integer-partial differential algebraic equations was solved simultaneously using an equation-oriented approach, which is considered faster and more robust than a sequential-modular one.[20] This approach has been applied successfully in previous works.[13,21] The gas-phase mass balance for a component (i) is shown in Equation (1) including accumulation, gas liquid mass transfer, convection, as well as axial and radial dispersion,

$$\varepsilon_G \frac{\partial C_{i,G}(t,z,r)}{\partial t} = -k_{GL}a_{GL}(C^*_{i,L} - C_{i,L}) - u_G \frac{\partial (C_{i,G}(t,z,r))}{\partial z} + \varepsilon_G D_{z,G}(z,r)\left(\frac{\partial^2 C_{i,G}(t,z,r)}{\partial z^2}\right) + \varepsilon_G D_{r,G}(z,r)\left(\frac{\partial^2 C_{i,G}(t,z,r,)}{\partial r^2} + \frac{1}{r}\frac{\partial C_{i,G}(t,z,r,)}{\partial r}\right) \quad (1)$$

The mass balance for the liquid bulk phase, Equation (2), shows that the accumulation equals a net effect of gas–liquid mass transfer, convection, as well as axial and radial dispersion. The liquid–solid mass transfer terms to supply reacting species from the liquid to the surface of the catalyst are included. The $k_{LS}a_{ls}(C_{i,L} - C_{i,s})$ term describes the mass transfer of hydrogen and sugar (e.g., arabinose) from the liquid bulk to the catalyst surface and the mass transfer of product (e.g., arabitol) from catalyst surface to the liquid bulk.

$$\varepsilon_L \frac{\partial C_{i,L}(t,z,r)}{\partial t} = +k_{GL}a_{GL}(C^*_{i,L} - C_{i,L}) - k_{LS}a_{LS}(C_{i,L} - C_{i,S}) - u_L \frac{\partial (C_{i,L}(t,z,r))}{\partial z} + \varepsilon_L D_{z,L}(z,r)\left(\frac{\partial^2 C_{i,L}(t,z,r)}{\partial z^2}\right) + \varepsilon_L D_{r,L}\left(\frac{\partial^2 C_{i,L}(t,z,r)}{\partial r^2} + \frac{1}{r}\frac{\partial C_{i,L}(t,z,r)}{\partial r}\right) \quad (2)$$

Another mass balance is required for the liquid film surrounding the catalyst layer in order to calculate concentrations of the liquid at the catalyst surface. This mass balance only includes the liquid–solid mass transfer and the reaction terms. A quasi-steady state is presumed to prevail in the liquid film: the mass transfer is compensated by the chemical reaction,

$$k_{LSi}a_{LS}(C_{i,L} - C_{i,s}) + \rho_{cat} r_{effi}(t,z,r) = 0 \quad (3)$$

In general, the effective component consumption/production reaction rate is the intrinsic rate multiplied by the effectiveness factor:

$$r_{effi} = ri\,\eta_{ei} \quad (4)$$

For thin catalyst layers and slow reactions $\eta_{ei} = 1$ can be assumed and the concentration gradients inside the catalyst layer are negligible. If the internal mass transfer in the pores of the catalyst layer has an impact on the observed kinetics, the effectiveness factor is obtained from the general reaction–diffusion model of the catalyst layer as will be shown in Section 2.2.

3.1 | Boundary conditions

The boundary conditions equations include the feed concentrations at the reactor inlet, as well as axial and radial derivatives of the component concentrations. The closed–closed boundary conditions of Danckwerts are applied at the reactor inlet and outlet. The boundary conditions are summarized below.

3.2 | Gas-phase boundary conditions

$$\text{Entrance: } C^{IN}_{i,G} = C_{i,G}(t,r) - (\varepsilon_G D_{z,G}(z,r)/(u_G L))(dC_{i,G}(t,r)/dz) \text{ at } z = 0 \quad (5a)$$

$$\text{Outlet: } \frac{\partial C_{i,G}(t,r)}{\partial z} = 0 \text{ at } z = 1 \quad (5b)$$

$$\text{Center: } \frac{\partial C_{i,G}(t,z)}{\partial r} = 0 \text{ at } r = 0 \quad (6a)$$

$$\text{Wall:}\ \frac{\partial C_{i,G}(t,z)}{\partial r}=0\ \text{ at }\ r=0 \tag{6b}$$

3.3 | Liquid-phase boundary conditions

$$\text{Entrance:}\ C_{i,L}^{IN}=C_{i,L}(t,r)-(\varepsilon_L D_{z,L}(z,r)/(u_L L))(dC_{i,L}(t,r)/dz)\ \text{ at }\ z=0 \tag{7a}$$

$$\text{Outlet:}\ \frac{\partial C_{i,L}(t,r)}{\partial z}=0\ \text{ at }\ z=1 \tag{7b}$$

$$\text{Center:}\ \frac{\partial C_{i,L}(t,z)}{\partial r}=0\ \text{ at }\ r=0 \tag{8a}$$

$$\text{Wall:}\ \frac{\partial C_{i,L}(t,z)}{\partial r}=0\ \text{ at }\ r=0 \tag{8b}$$

In particular, closed-closed boundary conditions were adopted to give a general validity to the model: depending on the Péclet number, the axial dispersion contribution can be dominant also at the reactor's inlet.

3.4 | Summary of balance equations

The reactor model consists of the gas-phase balances (1), the liquid-phase balances (2), the surface balances (3)–(4) as well as the boundary conditions (5a)–(8b). The gas- and liquid-phase balances (1)–(2) are parabolic partial differential equations (PDEs) which are coupled to the surface balance (3), which is a non-linear algebraic equation system (NLEs).

4 | ADVANCED MODEL

The simple model presented in the previous Section 2.1. is extended to a more advanced one by including the effect of the diffusion resistance inside the catalyst layer. This means that the mass balance Equation (3) will be replaced by a reaction–diffusion model for the porous catalyst layer.

The gas phase mass balance remains the same as stated by Equation (1).

4.1 | Liquid phase mass balance

In the advanced model, it is assumed that reactions occur within the solid catalyst layer. Thus, reacting components are diffusing first into the solid catalyst layer and then react on the active surface sites of the catalyst. Intrinsic reaction kinetics, effective diffusivities of the molecules inside the catalyst layer and the shape of the layer determine the net flux to/from the catalyst layer. Mass transfer flux to/from the catalyst layer is added on the very left-hand side of the correlation. The impact of such flux terms has been discussed in previous studies.[13,22,23]

$$\varepsilon_l\frac{\partial C_{i,L}(t,z,r)}{\partial t}=+k_{GL}a_{GL}(C^*_{i,L}-C_{i,L})-u_L\frac{\partial C_{i,L}(t,z,r)}{\partial z}+\varepsilon_L D_{z,L}\frac{\partial^2 C_{i,L}(t,z,r)}{\partial z^2}$$

$$+\varepsilon_L D_{r,L}\left(\frac{\partial^2 C_{i,L}(t,z,r)}{\partial r^2}+\frac{1}{r}\frac{\partial C_{i,L}(t,z,r)}{\partial r}\right)-\frac{f\,D_{eff,i}}{R_C{}^2}\left(\frac{\partial C_{i,s}(t,z,r,x)}{\partial x}\right)\Big|x=1 \tag{9}$$

where f is a correction factor, typically $f = 1$ or less. In fact, it can be shown that

$$f=(s+1)\left(\frac{\rho_B}{\rho_P}\right) \tag{10}$$

The background of this reasoning is explained in Appendix S1.

4.2 | Boundary conditions

Also here, the boundary conditions of Danckwerts are applied at the reactor inlet and outlet,

$$\text{Entrance:}\ C_{i,L}^{IN}=C_{i,L}(t,r)-(\varepsilon_L D_{z,L}(z,r)/u_L)(dC_{i,L}(t,r)/dz)\ \text{ at }\ z=0 \tag{11a}$$

$$\text{Outlet:}\ \frac{\partial C_{i,L}(t,r)}{\partial z}=0\ \text{ at }\ z=L \tag{11b}$$

$$\text{Center:}\ \frac{\partial C_{i,L}(t,z)}{\partial r}=0\ \text{ at }\ r=0 \tag{12a}$$

$$\text{Wall:}\ \frac{\partial C_{i,L}(t,z)}{\partial r}=0\ \text{ at }\ r=0 \tag{12b}$$

4.3 | Porous catalyst layer

The foam properties are inbuilt in parameters such as D_{eff}, ε_p, R_C, and ρ_{cat} in solid phase mass balance, Equation (13). A dimensionless coordinate, x, is taken in use, because the catalyst layer is very thin (<10 μm) and it is reasonable that the reactor and particle coordinates are not too different in the model implementation. The dimensionless coordinate is defined as $x = r_P/R_C$, where R_C is the catalyst layer thickness. Thus x is always between 0 and 1, where "1" corresponds to the outer surface of the catalyst layer.

$$\frac{\partial C_{i,s}(t,z,r,x)}{\partial t}=\frac{D_{eff,i}}{\varepsilon_p R_C^2}\left(\frac{\partial^2 C_{i,s}(t,z,r,x)}{\partial x^2}+\frac{s}{x}\frac{\partial C_{i,s}(t,z,r,x)}{\partial x}\right)$$

$$+\rho_{cat}\sum\left(v_{i,j}r_j(t,z,r,x)\right) \tag{13}$$

Due to the fact that the washcoat layer is very thin, the simple slab geometry can be used and then shape factor becomes 0. A shape factor, proposed by Bracconi et al.,[12] equals to 0.475 for foams with

circular strut cross-sectional shape and 0.810 for triangular shape. All three possibilities were considered in our modeling effort.

4.4 | Boundary conditions

The particle balance is coupled to the bulk liquid balance through the boundary condition, which states that the molar flux through the liquid film is equal to the molar flux in/out to/from the particle. This form is numerically stable even for the extreme case that $k_{i,LS}$ is large (i.e., no mass transfer limitation in the film surrounding the catalyst layer) and then $C_{i,s} = C_{i,L}$.

$$\frac{\partial C_{i,s}(t,z,r,x)}{\partial x} = 0 \text{ at } x = 0 \tag{14a}$$

$$C_{i,s} + \frac{D_{eff,i}}{k_{i,LS}} \frac{\partial C_{i,s}(t,z,r,x)}{R_C \, \partial x} = C_{i,L} \text{ at } x = 1 \text{ (outer surface of the layer)} \tag{14b}$$

4.5 | Effectiveness factor

The effectiveness factor of a component is by definition the ratio between the diffusion flux to/from the porous particle under diffusion-influence conditions and under the conditions of intrinsic kinetics. The effectiveness factors of the components are obtained from the integrated local rates inside the particle,

$$\eta_{ei} = \frac{(s+1)}{r_i(c_L)} \int_0^1 r_i x^s dx \tag{15}$$

where $r_i(c_L)$ denotes the rate calculated with the bulk-phase concentrations. The use of Equation (15) minimizes the numerical inaccuracies in the evaluation of the effectiveness factors, because it is based on the use of the integrated rates over the entire catalyst layer.[22,23] The effectiveness factor is obtained direct after that the particle model Equation (13) has been solved.

5 | PHYSICAL PROPERTIES

The most important physical properties needed in the model are density, viscosity and hydrogen solubility. Physiochemical properties of the components were calculated at the reactor entrance and kept constant throughout the reactor length and radius. This approximation is reasonable, as temperature variation is not considered, and the reaction conversions are very low. From the density and viscosity data, the liquid-phase diffusion coefficients can be calculated.

5.1 | Hydrogen solubility

The hydrogen solubility in the liquid phase is calculated by the following empirical expression proposed by Rivero et al.[24] and Sifontes et al.[25] The correlation Equation (16) for the hydrogen solubility is based on a large set of experimental data. The hydrogen pressure of the system is equal to P (bar), the temperature is T (K) and C_{H_2} (mol/L).

$$C_{H_2} = 9.35 \times 10^{-6} \cdot P_{H_2} \cdot T + 0.01447 \times 10^{-4} \cdot T^2 - 1.138 \times 10^{-3} \cdot T + 0.222 - 2.833 \times 10^{-3} \cdot P_{H_2} - 0.1481 \times 10^{-8} \cdot {P_{H_2}}^2 \tag{16}$$

5.2 | Liquid viscosity and molecular diffusivities

Equation (17) was implemented for the dynamic viscosity of the liquid phase. It is dependent on both concentration of the sugar solution and temperature. This correlation proposed by Rivero et al.[24] and Sifontes et al.[25] is based on density and kinematic viscosity measurements of sugar solutions. T (K) is the temperature of the system and x_A is the weight fraction of the sugar in the solution (wt%).

$$\mu_L[\text{Pa s}] = \exp\left(\frac{1.54 x_A}{T_L - 273} + 3.81 \times 10^{-4} x_A^2 - 1.10 \times 10^{-2} x_A - 2.85 + \frac{1.94 \times 10^2}{T_L - 273} - \frac{3.89 \times 10^3}{(T_L - 273)^2}\right) \times 10^{-3} \tag{17}$$

The molecular diffusivities of sugars, sugar alcohols and hydrogen in the liquid phase were calculated by using the Wilke and Chang correlation[26]:

$$D(\text{m}^2/\text{s}) = 7.4 \times 10^{-12} \frac{(xM)^{0.5} T}{\mu V_A^{0.6}} \tag{18}$$

5.3 | Gas and liquid densities

For the gas density, the ideal gas law is used. Liquid phase density was directly taken from the work of Rivero et al.[24] and Sifontes et al.[25], where the dependence of the liquid density with both temperature and composition is reported. T (°C) is the temperature of the system and x_A is the sugar concentration of the solution (wt%).

$$\rho\left(\frac{\text{kg}}{\text{m}^3}\right) = -0.008154 \cdot T \cdot x_A + 0.008424 \cdot {x_A}^2 + 4.797 \cdot x_A + 1065 - 1.627 \cdot T + 0.005412 \cdot T^2 \tag{19}$$

5.4 | Reaction rate expressions

Hydrogenation of arabinose (A) and galactose (G) to arabitol (A') and galactitol (G') is considered as a verification case of the model. For the hydrogenation of sugar mixtures (arabinose and galactose), a Langmuir–Hinshelwood expression with noncompetitive adsorption of hydrogen and the organic components was applied.[27–29] Furthermore, the quasiequilibrium hypothesis was applied on the adsorption steps, whereas it was assumed that the hydrogenation steps are rate-determining. The reaction kinetics was studied in detail in our

previous work,[30] where the underlying hypotheses of the reaction mechanism was thoroughly discussed, and the rate equations were derived.

The following rate equations was developed by our group for the sugar mixtures (arabinose (I) and galactose (II)) hydrogenation:

$$r_I = \frac{k_I c_A c_H}{(1 + K_A c_A + K_G c_G)\left(1 + \sqrt{K_H c_H}\right)^2} \tag{20}$$

$$r_{II} = \frac{k_I c_G c_H}{(1 + K_A c_A + K_G c_G)\left(1 + \sqrt{K_H c_H}\right)^2} \tag{21}$$

In case that only arabinose is hydrogenated, $K_G c_G$ is equal to 0 in the above equations. In our experiments the hydrogen pressure was constant, and $c_H/(1 + [K_H c_H]^{1/2})^2$ was constant, thus the Equations (20) and (21) are simplified to

$$r_I = \frac{k_I c_A}{1 + K_A c_A} \tag{22}$$

$$r_{II} = \frac{k_{II} c_G}{1 + K_A c_A} \tag{23}$$

The term $c_H/(1 + [K_H c_H]^{1/2})^2$ was approximated to be constant during the experiment, because very close to zero order behavior with respect to hydrogen has been observed in our previous studies of sugar hydrogenation on Ru/C catalysts (Sifontes et al.,[15] Araujo Barahona et al.[31]). The hydrogen solubility increases in aqueous sugar solutions as a function of temperature, because the polarity of water decreases with temperature. Detailed experimental studies on hydrogen solubility has been carried out by us (Sifontes et al.[25]) confirming this fact.

The Arrhenius law for the rate constants was expressed in a transformed form to suppress the correlation between the pre-exponential factor and the activation energy in the regression analysis,

$$k_I = k_{I\mathrm{ref}A} \exp\left[\frac{-E_{a\,I}}{R_g}\left(\frac{1}{T_s(t,z,r)} - \frac{1}{T_{\mathrm{ref}}}\right)\right] \tag{24}$$

$$k_{II} = k_{II\mathrm{ref}G} \exp\left[\frac{-E_{a\,II}}{R_g}\left(\frac{1}{T_s(t,z,r)} - \frac{1}{T_{\mathrm{ref}}}\right)\right] \tag{25}$$

where T_{ref} is the reference temperature of the experiments. The production and consumption rates of the components are obtained by the following equations:

$$r_A = -r_I \tag{26}$$

$$r_{A'} = r_I \tag{27}$$

$$r_G = -r_{II} \tag{28}$$

$$r_{G'} = r_{II} \tag{29}$$

$$r_H = -r_I - r_{II} \tag{30}$$

5.5 | Mass transfer coefficients

Under the actual experimental conditions, the liquid flow rate through the catalyst foam was low, which inevitably implies that the results are affected by the external mass transfer resistance at the outer surface of the foam. Therefore, correlations for mass transfer coefficients were considered and implemented in the model.

5.6 | Gas–liquid mass transfer coefficient

A correlation for gas–liquid mass transfer coefficient in open-cell foam bed packing has been proposed by Zapico et al.,[32]

$$\frac{a_{GL}\varepsilon_L}{a_p}\,\mathrm{Sh} = 0.0037 Re_L^{1.4}\, Sc_L^{0.5} \tag{31}$$

where the Sherwood number is $\mathrm{Sh} = d_p k_{GL} D_L^{-1}$ and k_{GL} is the gas–liquid mass transfer coefficient.

It is reported in the literature that in packed bed reactors, the global mass transfer coefficient is expected to increase with the liquid superficial velocity but to show little variation with the gas superficial velocity. A similar trend has been reported for packed beds with open cell foams.[32–35]

5.7 | Liquid–solid mass transfer coefficient

The liquid–solid mass transfer coefficient (k_{LS}) was calculated by using Equation (33) proposed by Cognet et al.,[36]

$$k_{LS} = \left[Re_{L_{\mathrm{eq}}}.\tau.Sc_L^{1/3} - 16.9 \cdot \frac{d_{\mathrm{hyd}}}{d_R} Re_{L_{\mathrm{eq}}}{}^{\beta} \cdot Sc_L^{1/3}\right] \cdot \frac{D_L}{d_{\mathrm{hyd}}} \tag{32}$$

$\beta = 0.28$ for a 20 PPI foam and $\beta = 0.25$ for a 45 PPI foam was proposed by Lali et al.[37]

τ is the tortuosity of the foam structure and was calculated applying Equation (33) which was proposed by Plessis et al.[38]:

$$\frac{1}{\tau} = \frac{3}{4\varepsilon} + \frac{\sqrt{9 - 8\varepsilon}}{2\varepsilon} \cdot \cos\left\{\frac{4\pi}{3} + \frac{1}{3}\cos^{-1}\left[\frac{8\varepsilon^2 - 36\varepsilon + 27}{(9 - 8\varepsilon)^{1.5}}\right]\right\} \tag{33}$$

An alternative formula for the calculation of k_{LS} has been proposed by Mohammed et al.[4] for tubular reactors with solid foam packings,

$$\frac{\varphi Sh}{Sc^{1/3}} = a Re_L{}^b\, Re_G{}^c \left(a_s d_w \frac{1 - \varepsilon}{\varepsilon}\right)^d \tag{34}$$

5.8 | Liquid-holdup

The conditions of our experiments (very low gas and liquid superficial velocities) corresponded to the trickle flow regime as confirmed by the information available in the previous literature.[30,39,40] To calculate the total liquid hold-up, as well as the static and dynamic hold-ups

were estimated from Equations (35) and (36). Both correlations were proposed by Zalucky et al.[35] for solid foams. The dynamic holdup is based on the Galileo and Reynolds numbers while the static holdup is based on the Eötvös number.

$$\varepsilon_{L,\mathrm{dyn}} = 4.44 Re_L^{0.56} \cdot Ga_L^{-0.42} \tag{35}$$

$$\varepsilon_{L,S} = \frac{1}{2.62 + 3.72 \cdot E\ddot{o}^*} \tag{36}$$

where the Eötvös number ($E\ddot{o}^*$) is

$$E\ddot{o}^* = \frac{\rho_L \cdot g \cdot d_e^2}{\sigma_L} \tag{37}$$

and the Galileo number (Ga_L) is:

$$Ga_L = \frac{g d_e^3}{\upsilon_L^2}. \tag{38}$$

5.9 | Pressure drop

The experimental and simulated data of pressure drop are compared in Figure 3. The simulations were based on Equation (39). The pressure drop experiments were conducted with carbon coated aluminum foams at the liquid volumetric flow rate of 0.5 ml/min and different gas volumetric flow rates (0–302 ml/min). The continuously operated tubular reactor was packed with foams as illustrated in Figure 1, with one uncoated foam at the top and two coated foams at the bottom. The gas used was argon and the liquid was distilled water. The gas flow rate was controlled by a mass flow controller (Brooks 5850S) and the liquid was pumped to the reactor with an HPLC pump (Knauer Smartline 100). Downward concurrent gas and liquid flows were applied, and the gas and liquid passed through the foams in the sequence: uncoated foam—first coated foam—second coated foam. A pressure sensor (Keller PR21S sensor with the range 0–2.5 bar [g] and output 4–20 mA) was located upstream of the reactor in the gas feed line. A CAL9500P controller (West Control solutions) was used to convert the 4–20 mA signal to a pressure value. The following correlation for the estimation of the pressure drop in a tubular reactor with open cell foam packing has been proposed by Mohammed et al.[3] and it was used in this work:

$$\frac{dP}{dz} = \rho_L g \left(a_1 Re_L^{b_1} Re_G^{c_1}\right) \left(a_s d_w \frac{1-\varepsilon}{\varepsilon}\right)^{d_1} \tag{39}$$

where d_w is the window (pore) diameter, $a_1 = 21.56$, $b_1 = 0.15$, $c_1 = 3.45$, and $d_1 = 9.80$.

In the existing literature, different characteristic lengths have been used for simulating the pressure drop. Saber et al.[41] used cell diameter as a characteristic length, Mohammed et al.[3] used window diameter, and Edouard et al.[39] and Giani et al.[40] used strut diameter.

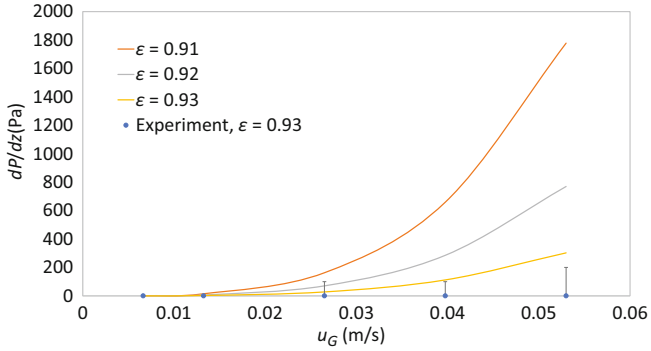

FIGURE 3 Experimental pressure drop data versus simulations with different foam porosities

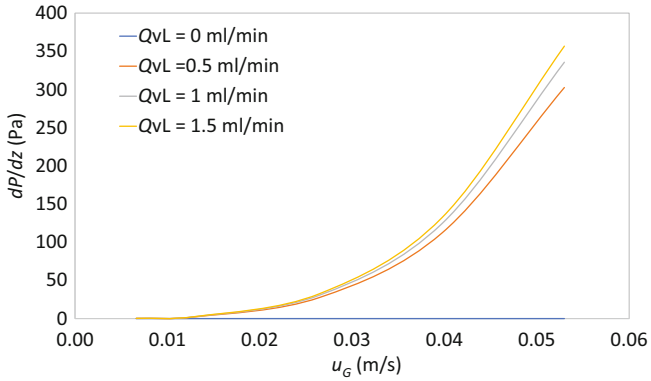

FIGURE 4 Pressure drop data with different gas and liquid superficial velocities

According to the experimental results obtained from the pressure drop measurements (Figures 3 and 4), even if inaccurate, we used the cell diameter as a characteristic length for simulating the pressure drop and the liquid hold up.

The results display that changing the foam porosity has a strong effect on the pressure drop. An aluminum foam with a porosity of 0.93 was used for preparing the carbon coated foam catalyst. Comparing the experimental data with the simulation results indicates that the foam porosity was decreased to 0.916 because of the coating. Figure 4 displays the pressure drop experiments with different liquid (0.5–1.5 ml/min) and gas (0–302 ml/min) volumetric flow rates. The trends are expected.

5.10 | Axial and radial dispersion coefficients

Saber et al.[41] have proposed a correlation for the Péclet number (Pe) in open cell foams. The concept was based on the use of the cell diameter (d_c). The Péclet number to calculate the axial dispersion coefficient is obtained as follows

$$Pe'_L = \frac{u_L d_c}{D_{z,L}} \tag{40}$$

where d_c is the cell diameter, equivalent particle diameter.

$$Pe'_L = aRe^b \tag{41}$$

where $a = 0.042$, $b = 0.5$ for open cell foams according to Hochman and Effron.[42] The Péclet number used in the axial dispersion model is based on the reactor length,

$$Pe_L = \frac{u_L L}{D_{z,L}} \tag{42}$$

And we get

$$Pe_L = \frac{Pe'_L L}{d_c} \tag{43}$$

Finally, the axial dispersion coefficient is calculated from

$$D_{z,L} = u_L \frac{L}{Pe_L}, \tag{44}$$

For the gas-phase axial dispersion coefficient, an analogous treatment is possible, giving:

$$D_{z,G} = u_G \frac{L}{Pe_G}, \tag{45}$$

The corresponding radial dispersion coefficient can be taken as a fraction of the axial one. As reported by Truong et al.[43] solid foam packing shows similar behavior of packed beds. Russo et al.[13] proposed that the value of radial dispersion coefficient is one third of the axial one for packed bed reactors. As a matter of fact, radial dispersion for systems not very much deviating from ideality are less influent than axial dispersion. A sensitivity analysis was conducted on this parameter, observing that its influence is only secondary on the simulation results.

TABLE 1 Geometrical properties of open cell foam with 0.93 porosity

d_c [mm][a]	d_w [mm][a]	S_V [m^{-1}][a]	d_S [mm][a]	Washcoat thickness [μm]
1.85	0.95	954	0.2	~7

[a]Values were adopted from Amberosio et al. [39].

6 | RESULTS AND DISCUSSION

6.1 | Experimental data

The dynamic models presented in section two were implemented to describe the sugar mixtures (arabinose and galactose) hydrogenation experiments carried out in a trickle bed with a cylindrical solid foam packing as a case study. The experimental data was studied in detail in our previous works.[8,30] Geometrical features listed in Table 1 were adopted from Amberosio et al.[44] as they used the same aluminum open cell foam, and the washcoat thickness layer value was adopted from Lali et al.[36] as they carried out the same method for coating aluminum open cell foams as we applied.

Figure 5 displays arabinose and galactose conversions as a function of temperature for experimental and calculated data for both simple and advanced models. Both models were capable to predict the conversions successfully. Hydrogenation experiments of binary sugar mixtures were performed with inlet molar ratios of 1:1 and 1:2. Experiments were carried out with liquid flow rate of 0.5 ml/min and gas (hydrogen) flow rate of 25 ml/min at different temperatures 90°C–120°C. The experimentally recorded sugar conversions on the figures are averages from multiple samples. The selectivity toward sugar alcohols was always very high, typically exceeding 95%.

6.2 | Parameter estimation results and discussion

Parameter estimation activities were conducted imposing isothermal condition, as in our previous investigation, we demonstrated that for arabinose hydrogenation the temperature increase due to the exothermicity of the reaction was not significant, leading only to small temperature gradients.[13]

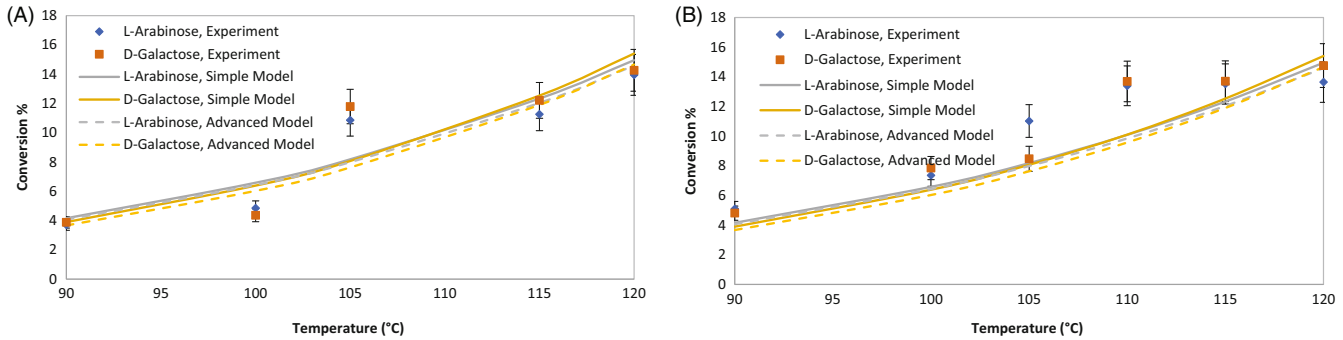

FIGURE 5 Conversion of sugar mixtures as a function of temperature. Inlet molar ratio (A) 1:1, (B) 1:2.

The parameter estimation results for both models, including the activation, kinetic constants calcylated at the reference temperature, together with the related 95% confidence intervals (CI), and correlation matrixes are given in Tables 2–4. As revealed, in all cases the confidence intervals fall within 10% error, indicating a good accuracy of the parameters. The correlation matrixes show no significant correlation between the estimated parameters in any of the models. R^2 for both the simple and advance models are, respectively, 0.87 and 0.90, indicating a good fit. Corresponding parity plots for both models (the advanced and simple ones) are displayed in Figure 6. There are good agreements between calculated (both models) and experimental data. The average error for the parity plots was about 16%.

In Figures 7 and 8, the sugar mixture conversions and reaction rates along both the reactor length and radius are visualized. No concentration gradients, thus also no conversion and reaction rate gradients, appeared in the radial direction, and the gradients are virtually linear with the length of the reactor, which can be explained with the relatively low conversions in the tubular reactor.

6.3 | Sensitivity analysis

To examine the capabilities of our models, a sensitivity analysis was performed and the effect of the kinetic parameters and operation conditions on the arabinose and galactose conversions was studied. Figure 9 shows the effect of different kinetic parameters such as activation energy (E_a) and rate constant at the reference temperature (k_{lref}) on the conversion of the sugar mixtures. As expected, the sugar conversion increased with increasing the activation energy and reference rate constant. The trends are rather linear. In the first case, starting from a sugar conversion of 10%, it is possible to improve it to 18% increasing 100% times the kinetic constant or the space time in the reactor.

The effect of increasing the reference rate constant on the arabinose and galactose concentrations was studied in the middle and at the end of the reactor. The catalyst layer thickness of 600 μm was used as an example and results are displayed in Figure 9. The results show that as the reference rate constant increases, the concentration of arabinose and galactose at the catalyst surface decreases which consequently result in an increase of the concentration gradient in the catalyst layer. This result surely demonstrates that the proposed model is very flexible, as it can simulate both ideal cases, characterized by a catalyst effectiveness factor approaching to the unity, and systems dominated by high intraparticle diffusion limitations. This aspect is surely a point of strength in the model utilization also for other chemical systems.

The effects are better highlighted by reporting by displaying a dimensionless concentration versus the layer position. In this way, at the catalyst surface, the dimensionless concentration is always equal to 1. Figure 10C) shows the calculated profiles at the catalyst surface,

TABLE 4 Correlation matrix of the estimated parameters in the advanced model

$s = 0$		E_{al}	E_{all}	k_{lrefA}	k_{llrefG}
	E_{al}	1			
	E_{all}	+0.1	1		
	k_{lrefA}	−0.1	+0.1	1	
	k_{lrefG}	+0.1	−0.2	+0.1	1
$s = 0.475$		E_{al}	E_{all}	k_{lrefA}	k_{llrefG}
	E_{al}	1			
	E_{all}	+0.1	1		
	k_{lrefA}	−0.1	+0.1	1	
	k_{lrefG}	+0.1	−0.1	+0.1	1
$s = 0.81$		E_{al}	E_{all}	k_{lrefA}	k_{llrefG}
	E_{al}	1			
	E_{all}	+0.1	1		
	k_{lrefA}	−0.1	+0.1	1	
	k_{lrefG}	+0.1	−0.1	+0.1	1

TABLE 2 Parameters estimation results for the simple model, and respective correlation matrix (CM)

Parameters	Estimated value ± 95% CI	CM	E_{al}	E_{all}	k_{lrefA}	k_{llrefG}
$E_{a\,l}$ [J/mol]	(5.36 ± 0.36) E+04	E_{al}	1			
$E_{a\,ll}$ [J/mol]	(5.76 ± 0.41) E+04	E_{all}	−0.1	1		
$k_{lrefA}s^{-1}$	(5.89 ± 0.20) E−07	k_{lrefA}	−0.1	+0.1	1	
$k_{llrefG}s^{-1}$	(5.81 ± 0.21) E−07	k_{lrefG}	+0.1	−0.1	−0.1	1

TABLE 3 Parameters estimation results for the advanced model with different shape factors (s)

Parameters	Estimated value ± 95% CI $s = 0$	Estimated value ± 95% CI $s = 0.475$	Estimated value ± 95% CI $s = 0.81$
E_{al} [J/mol]	(5.5 ± 0.4) E+04	(5.3 ± 0.4) E+04	(5.3 ± 0.3) E+04
E_{all} [J/mol]	(5.6 ± 0.4) E+04	(5.8 ± 0.4) E+04	(5.6 ± 0.4) E+04
$k_{lrefA}s^{-1}$	(5.8 ± 0.2) E−07	(8.8 ± 0.3) E−07	(1.12 ± 0.03) E−06
$k_{llrefG}s^{-1}$	(6.1 ± 0.2) E−07	(8.4 ± 0.3) E−07	(1.08 ± 0.03) E−06

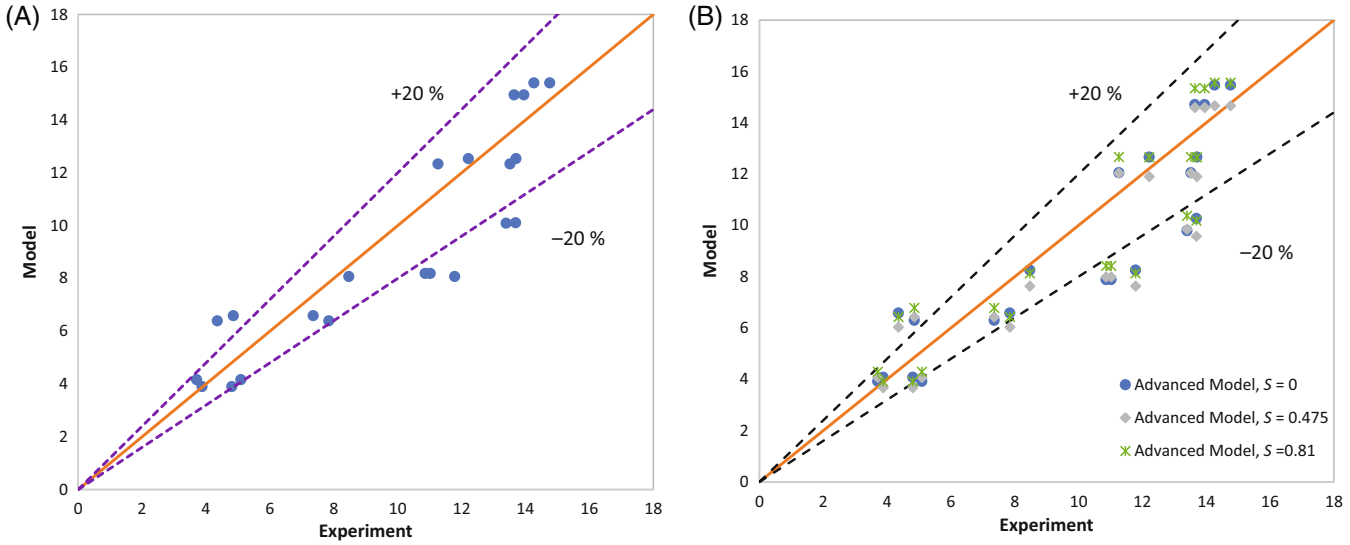

FIGURE 6 Parity plots of experimental data—simple (A) and advanced model (B).

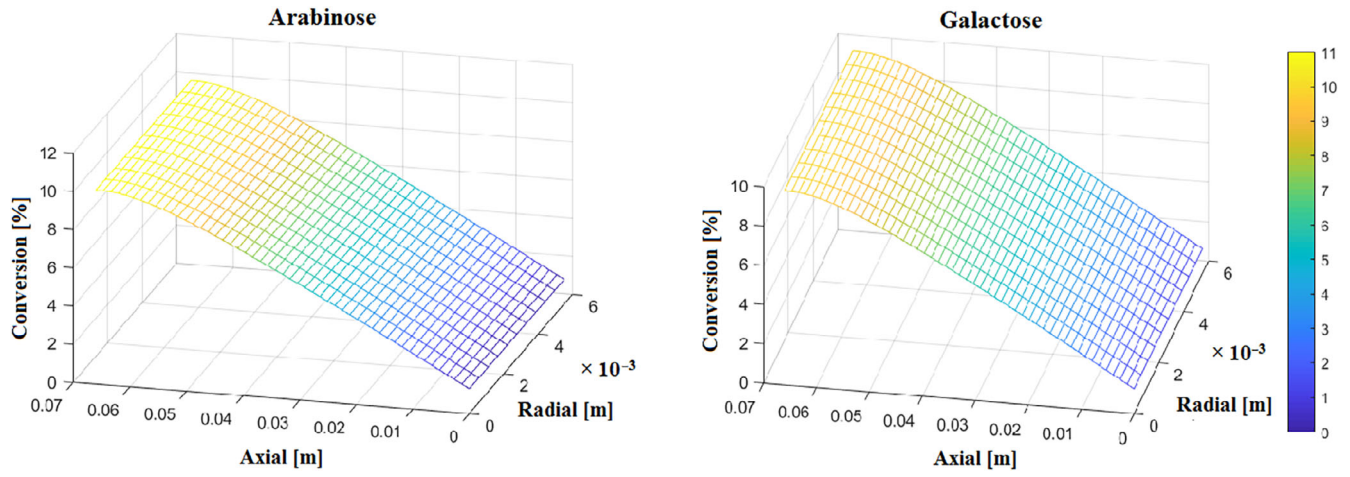

FIGURE 7 Arabinose and galactose conversions in axial and radial directions

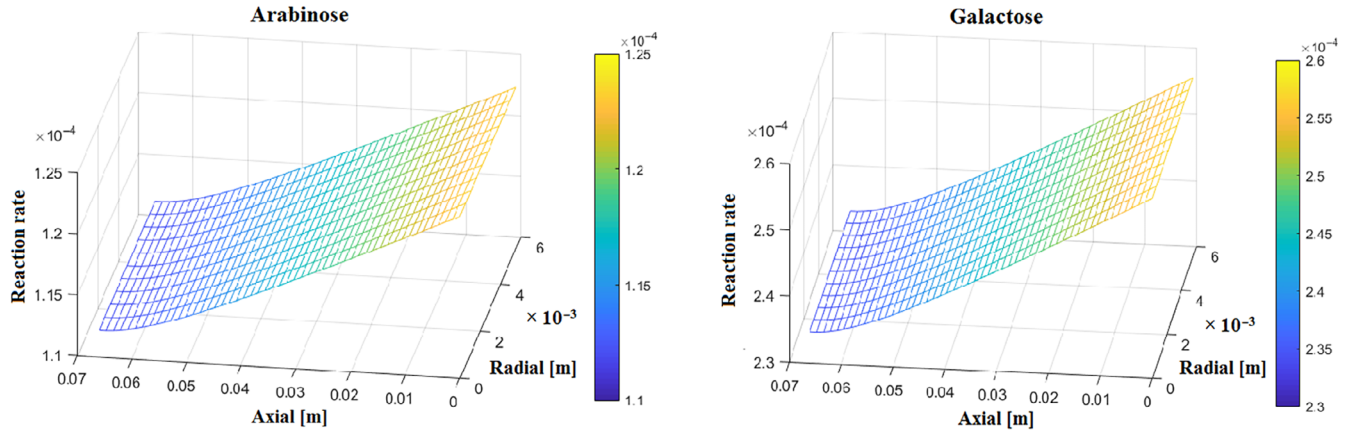

FIGURE 8 Reaction rates of sugar mixtures

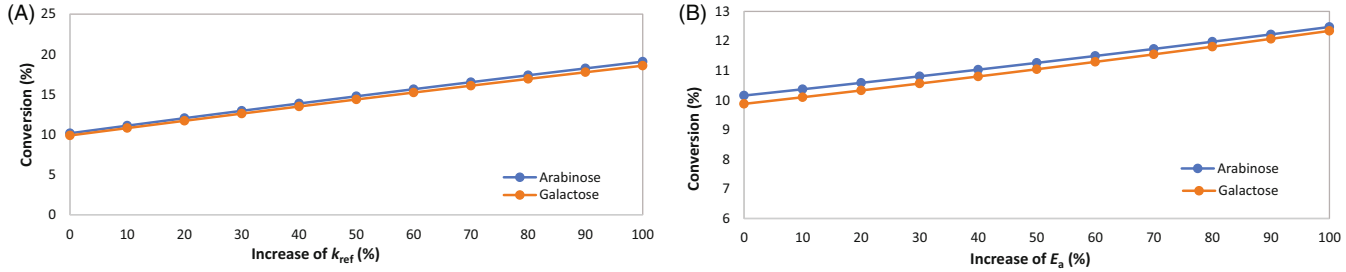

FIGURE 9 Conversions of sugars as a function of the reference rate constant (A) and activation energy; (B) with a washcoat thickness of 7 μm.

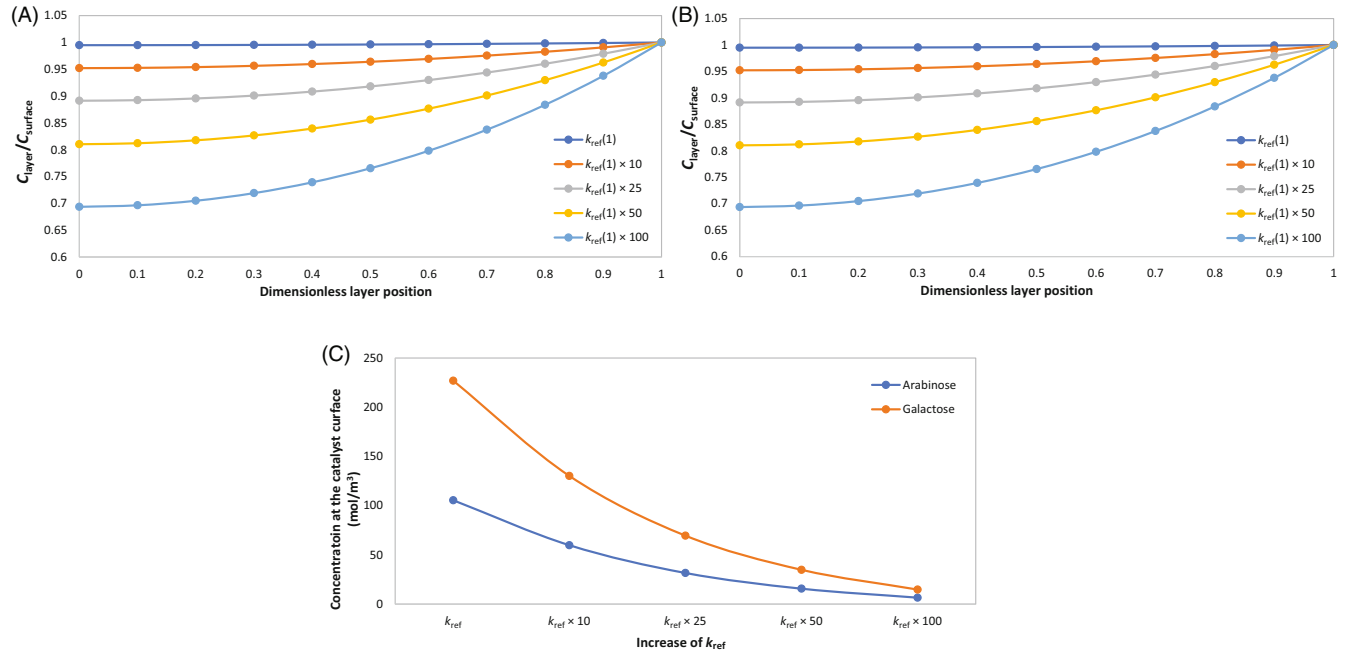

FIGURE 10 Effect of increasing the reference rate constant on the arabinose concentrations in the middle of the reactor (A) and at the end of the reactor (b) with washcoat thickness of 600 μm.

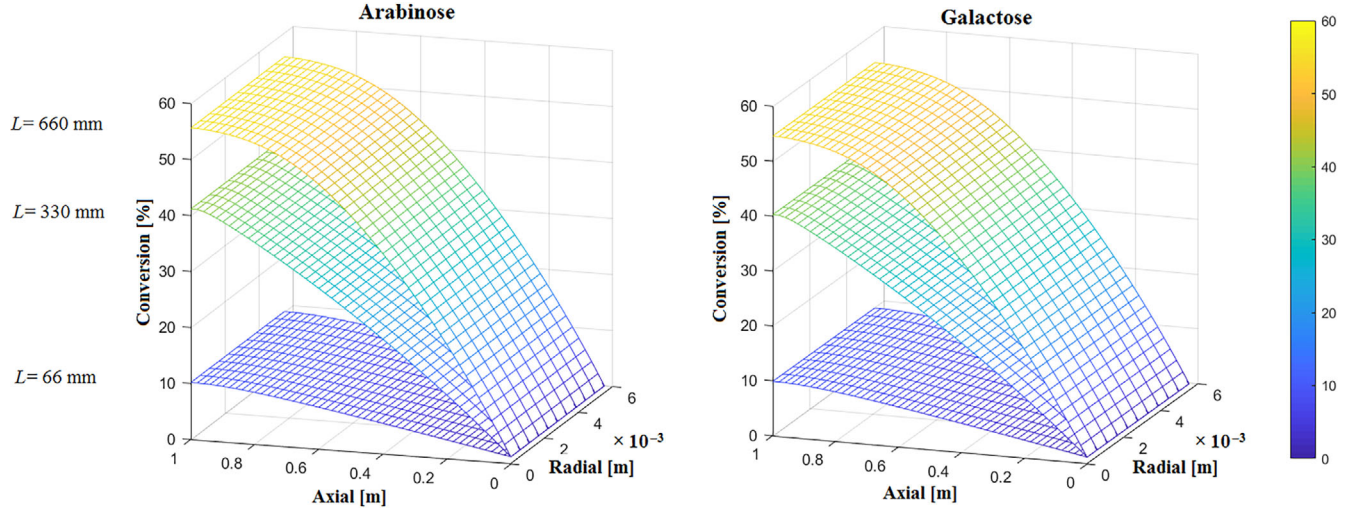

FIGURE 11 Conversions of arabinose and galactose as a function of the reactor length

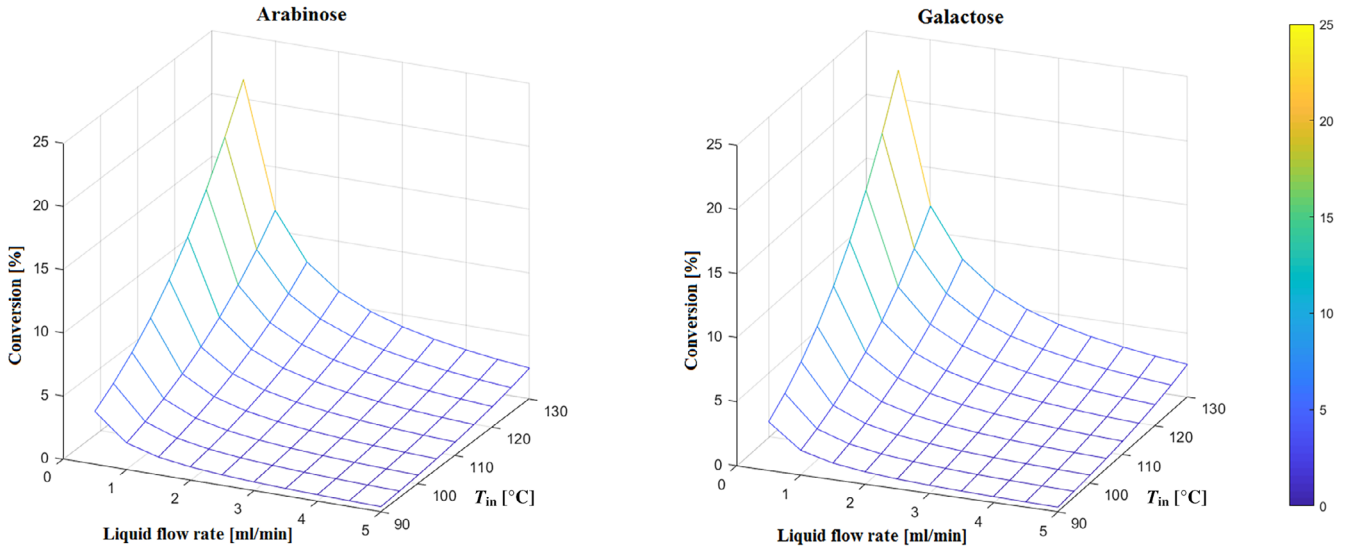

FIGURE 12 Conversions of arabinose and galactose as a function of the liquid flow rate and inlet temperature

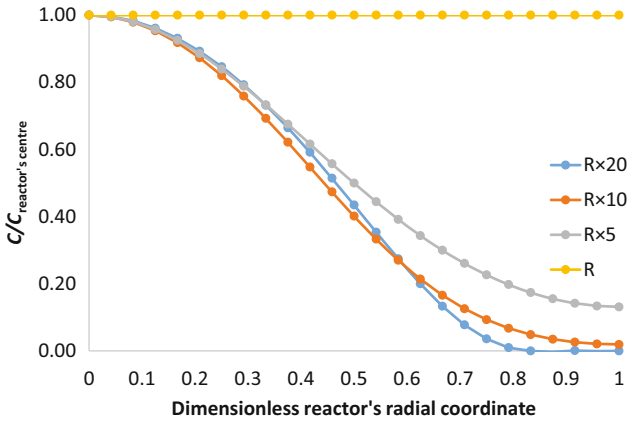

FIGURE 13 Dimensionless concentration of arabinose as a function of the dimensionless reactor radius for an industrial scale reactor. Simulations are collected at the reactor's center

showing a decreasing value with the increase of the reference kinetic constant.

The effect of increasing the reactor length on the sugar conversions was studied in Figure 11, which shows that the conversions increased in line with the reactor length. No radial gradients are predicted even for longer reactors. The conversions as a function of the liquid flow rate and the inlet temperature are illustrated in Figure 12. The conversions increased strongly as the temperature increased and they were at its highest with low flow rates such as 0.5 ml/min. The results indicate that for obtaining higher conversions with a small reactor volume like the one we used in our experimental studies, it is better to use low liquid flow rates and high temperatures.

As revealed by the previous figures, reactors radial profiles are rather flat, fact reasonable as the experiments were conducted in a lab-scale reactor where radial effects are frequently suppressed due both to the dimension of the reactor and to the chosen reaction conditions. Therefore, the model can be considered general, as includes radial dispersion term both in the mass balances and in the boundary conditions. To test the flexibility of the model, several simulations were conducted to check what could be the concentration gradients along the radial direction for an industrial scale reactor ($L = 5$ m), selecting a pipe radius between the radius of the lab scale reactor used in the present work and 20 times its value (see Figure 13).

It is evident that concentration gradients are surely important for larger reactors, as expected, and that the model can simulate a wide variety of different situations, ranging from flat to high gradients.

7 | CONCLUSIONS

Advanced dynamic isothermal models for three-phase catalytic tubular reactors with solid foam packings were developed and implemented. The gas, liquid and solid phase mass balances included the individual terms such as internal diffusion, gas–liquid and liquid solid mass transfer and intrinsic kinetics for solid foam packings. Two versions of the mathematical model were considered in detail: a simplified model, where the gas–liquid and liquid–solid mass transfer resistance were included and an advanced model, which included the mass transfer resistance in the pores of the catalyst layer.

Previously obtained catalytic hydrogenation results of binary sugar mixtures (arabinose and galactose) were utilized in this modeling and simulation study. The kinetic parameters of the model were estimated with a good accuracy. As a summary, we can conclude that according to Figures 5–12, the model for the solid foam proposed in this work was capable of predicting the effect of different kinetic and transport phenomena under various operation conditions. The models

described here are applicable for other three-phase studies in catalytic tubular reactors packed with solid foams.[45–50]

ACKNOWLEDGMENT

The present work was financed by Finnish Cultural Foundation, Neste-Fortum Foundation and Rector of Åbo Akademi University (Ali Najarnezhadmashhadi) and Academy of Finland, Academy Professor grant 319002 (Tapio Salmi). The economic support is gratefully acknowledged. Open Access Funding provided by Universita degli Studi di Napoli Federico II within the CRUI-CARE Agreement.

AUTHOR CONTRIBUTIONS

Ali Najarnezhadmashhadi: Data curation (equal); investigation (lead); methodology (equal); software (equal); validation (equal); writing – original draft (equal); writing – review and editing (equal). **Catarina Braz:** Data curation (equal); formal analysis (equal); investigation (equal); methodology (equal); software (lead); validation (equal); writing – original draft (equal); writing – review and editing (equal). **Vincenzo Russo:** Conceptualization (lead); data curation (equal); formal analysis (lead); methodology (lead); project administration (equal); software (lead); supervision (lead); visualization (equal); writing – original draft (equal); writing – review and editing (equal). **Kari Eränen:** Data curation (equal); investigation (equal); resources (equal); supervision (equal); writing – original draft (equal); writing – review and editing (equal). **Henrique Matos:** Conceptualization (equal); funding acquisition (lead); project administration (equal); supervision (equal); writing – original draft (equal); writing – review and editing (equal). **Tapio Salmi:** Conceptualization (lead); funding acquisition (lead); project administration (lead); supervision (equal); writing – original draft (equal); writing – review and editing (equal).

DATA AVAILABILITY STATEMENT

Data sharing not applicable - no new data generated.

NOTATION

a_p	packing specific surface area [m^2/m^3]
a_{GL}	volume-specific gas–liquid interfacial surface area [m^2/m^3]
a_{LS}	mass transfer area between liquid phase and foam catalyst [m^2/m^3] $a_{LS} = a_S\epsilon_L$
a_S	volume-specific geometrical surface area of foam substrate [m^2/m^3]
C_i^*	component i saturation concentration [mol/m^3]
$C_{i,\mathrm{ref}}^*$	component i saturation concentration at reference pressure [mol/m^3]
$C_{i,j}$	concentration of component i in phase j [mol/m^3]
$C_{i,j}^{\mathrm{IN}}$	initial concentration of component i in phase j [mol/m^3]
$D_{\mathrm{eff},i}$	effective diffusivity of component i in water [m^2/s]
$D_{i,j}$	molecular diffusivity of i in phase j [m^2/s]
$D_{r,j}$	radial dispersion coefficient of phase j [m^2/s]
$D_{z,i}$	axial dispersion coefficient of phase j [m^2/s]
dc	cell diameter [m]
ds	strut diameter [m]
d_w	window (pore) diameter [m]
d_{hyd}	hydraulic diameter [m] $d_{\mathrm{hyd}} = 4\varepsilon a_S^{-1}$
d_{eq}	corrected equivalent diameter [m]
E_a	activation energy [J/mol]
$Eö^*$	modified Eötvös number [−]
f	correction factor [−]
Fr_j	Froude number
Ga_L	Galileo number [−]
i	component i
j	phase j = G (gas), L (liquid), p (particle)
k	kinetic constant [$mol/(g_{cat}\ s)$]
K_A	arabinose adsorption parameter [m^3/mol]
K_G	galactose adsorption parameter [m^3/mol]
K_{H2}	hydrogen adsorption parameters [m^3/mol]
k_{GL}	gas liquid mass transfer coefficient for component i [s^{-1}]
k_{LS}	liquid solid mass transfer coefficient for component i [s^{-1}]
k_{ref}	kinetic constant at reference temperature [$mol/(g_{cat}\ s)$]
L	reactor length [m]
P	pressure [Pa]
Pe_L	Peclet Number of the phase j [−]
R	reactor radius [m]
r	radial location [m]
R_C	catalyst layer thickness [μm]
Re_L	Reynolds number for the liquid phase [−] $Re_L = \frac{\rho_L u_L d_{eq}}{\mu_L}$
R_g	ideal gas constant [J/(K mol)]
r_{eff}	effective reaction j rate [mol/(g s)]
r_j	reaction j rate [mol/(g s)]
r_p	particle radial location [m]
S_V	packing specific surface area [m^2/m^3]
s	shape factor [−]
Sh	Sherwood number [−]
Sc_L	Schmidt number [−] $S_{cL=}\mu_j D_L^{-1}\rho_j^{-1}$
t	time [s]
T_j	temperature of phase j [K]
T_{ref}	reference temperature [378 K]
u_j	velocity of the phase j [m/s]
V	reactor volume [m^3]
V_P	particle volume [m^3]
We_j	Weber number of the phase j [−]
x	dimensionless coordinate [−]
x_A	arabinose initial concentration [wt.%]
z	axial location [m]

Greek symbols

ϵ_B	hydraulic void fraction [−]
ϵ_j	holdup of phase j [−]
$\epsilon_{L,\mathrm{dyn}}$	dynamic liquid holdup [−]
$\epsilon_{L,s}$	static liquid holdup [−]
η	effectiveness factor [−]
η_j	viscosity of phase j [Pa s]
ρ_j	density of phase j [kg/m^3]
ρ_{cat}	catalyst concentration referred to liquid phase [kg/m^3]
ρ_{bed}	catalyst bulk density [kg/m^3]
σ_L	liquid surface tension [N/m]
τ	tortuosity [−]

Abbreviations

A	arabinose
A'	arabitol
H_2	hydrogen
dyn	dynamic
G	galactose
G'	galactitol
HPLC	high performance liquid chromatography
PDE	partial differential equation
NLEs	non-linear algebraic equation system

ORCID

Vincenzo Russo https://orcid.org/0000-0002-1867-739X
Tapio Salmi https://orcid.org/0000-0002-9271-7425

REFERENCES

1. Edouard D, Lacroix M, Pham C, Mbodji M, Pham-Huu C. Experimental measurements and multiphase flow models in solid SiC foam beds. *AIChE J*. 2008;54(11):2823-2832. doi:10.1002/aic.11594
2. Stemmet CP, Jongmans JN, van der Schaaf J, Kuster BFM, Schouten JC. Hydrodynamics of gas–liquid counter-current flow in solid foam packings. *Chem Eng Sci*. 2005;60(22):6422-6429. doi:10.1016/j.ces.2005.03.027
3. Mohammed I, Bauer T, Schubert M, Lange R. Hydrodynamic multiplicity in a tubular reactor with solid foam packings. *Chem Eng J*. 2013;231:334-344. doi:10.1016/j.cej.2013.07.024
4. Mohammed I, Bauer T, Schubert M, Lange R. Liquid–solid mass transfer in a tubular reactor with solid foam packings. *Chem Eng Sci*. 2014;108:223-232. doi:10.1016/j.ces.2013.12.016
5. Twigg MV, Richardson JT. Theory and applications of ceramic foam catalysts. *Chem Eng Res Des*. 2002;80(2):183-189. doi:10.1205/026387602753501906
6. Grosse J, Kind M. Hydrodynamics of ceramic sponges in countercurrent flow. *Ind Eng Chem Res*. 2011;50(8):4631-4640. doi:10.1021/ie101514w
7. Stemmet CP. Gas-liquid solid foam reactors: hydrodynamics and mass transfer. *Chem React Eng*. 2008. doi:10.6100/IR635735
8. Najarnezhadmashhadi A, Eränen K, Engblom S, Aho A, Murzin D, Salmi T. Continuous hydrogenation of monomeric sugars and binary sugar mixtures on a ruthenium catalyst supported by carbon-coated open-cell aluminum foam. *Ind Eng Chem Res*. 2020;59(30):13450-13459. doi:10.1021/acs.iecr.0c01565
9. Campbell LE. Catalyst for the production of nitric acid by oxidation of ammonia. US Patent 5336656A; 1993.
10. Hamidipour M, LarachiF RZ. Monitoring filtration in trickle beds using electrical capacitance tomography. *Ind Eng Chem Res*. 2009;48(3):1140-1153. doi:10.1021/ie800810t
11. Mohammed I, Bauer T, Schubert M, Lange R. Gas–liquid distribution in tubular reactors with solid foam packings. *Chem Eng Process Process Intensif*. 2015;88:10-18. doi:10.1016/j.cep.2014.11.016
12. Bracconi M, Ambrosetti M, Maestri M, Groppi G, Tronconi E. A fundamental investigation of gas/solid mass transfer in open-cell foams using a combined experimental and CFD approach. *Chem Eng J*. 2018;352:558-571. doi:10.1016/j.cej.2018.07.023
13. Russo V, Kilpiö T, Di Serio M, et al. Dynamic non-isothermal trickle bed reactor with both internal diffusion and heat conduction: sugar hydrogenation as a case study. *Chem Eng Res Des*. 2015;102:171-185. doi:10.1016/j.cherd.2015.06.011
14. Durante D, Kilpiö T, Suominen P, et al. Modeling and simulation of a small-scale trickle bed reactor for sugar hydrogenation. *Comput Chem Eng*. 2014;66:22-35. doi:10.1016/j.compchemeng.2014.02.025
15. Sifontes Herrera VA, Oladele O, Kordás K, et al. Sugar hydrogenation over a Ru/C catalyst. *J Chem Technol Biotechnol*. 2011;86(5):658-668. doi:10.1002/jctb.2565
16. Al-Dahhan MH, Larachi F, Dudukovic MP, Laurent A. High-pressure trickle-bed reactors: a review. *Ind Eng Chem Res*. 1997;36(8):3292-3314. doi:10.1021/ie9700829
17. Atta A, Roy S, Nigam KDP. A two-phase Eulerian approach using relative permeability concept for modeling of hydrodynamics in trickle-bed reactors at elevated pressure. *Chem Eng Res Des*. 2010;88(3):369-378. doi:10.1016/j.cherd.2009.06.011
18. Kuzeljevic ZV, Dudukovic MP. Computational modeling of trickle bed reactors. *Ind Eng Chem Res*. 2012;51(4):1663-1671. doi:10.1021/ie2007449
19. Wang Y, Chen J, Larachi F. Modelling and simulation of trickle-bed reactors using computational fluid dynamics: a state-of-the-art review. *Can J Chem Eng*. 2011;91(1):136-180. doi:10.1002/cjce.20702
20. PSE. Concepts - Equation-oriented simulation and modelling. Psenterprisecom; 2019. https://www.psenterprise.com/concepts/equation-oriented
21. Braz CG, Mendes A, Rocha J, Alvim R, Matos HA. Model of an industrial multitubular reactor for methanol to formaldehyde oxidation in the presence of catalyst deactivation. *Chem Eng Sci*. 2019;195:347-355. doi:10.1016/j.ces.2018.09.033
22. Toppinen S, Rantakylä T-K, Salmi T, Aittamaa J. Kinetics of the liquid-phase hydrogenation of benzene and some monosubstituted alkylbenzenes over a nickel catalyst. *Ind Eng Chem Res*. 1996;35(6):1824-1833. doi:10.1021/ie9504314
23. Toppinen S, Rantakylä T-K, Salmi T, Aittamaa J. Kinetics of the liquid phase hydrogenation of di- and trisubstituted alkylbenzenes over a nickel catalyst. *Ind Eng Chem Res*. 1996;35(12):4424-4433. doi:10.1021/ie950636c
24. Rivero DE. *Physical Properties of Sugar Solutions and Hydrogenation Reactions of Sugar into Sugar Alcohols over Ru/C Monolithic Catalysts*. Åbo Akademi University; 2009.
25. Sifontes Herrera VA, Rivero Mendoza DE, Leino A-R, et al. Sugar hydrogenation in continuous reactors: from catalyst particles towards structured catalysts. *Chem Eng Process Process Intensif*. 2016;109:1-10. doi:10.1016/j.cep.2016.07.007
26. Wilke CR, Chang P. Correlation of diffusion coefficients in dilute solutions. *AIChE J*. 1955;1(2):264-270. doi:10.1002/aic.690010222
27. Mikkola J-P, Vainio H, Salmi T, Sjöholm R, Ollonqvist T, Väyrynen J. Deactivation kinetics of Mo-supported Raney Ni catalyst in the hydrogenation of xylose to xylitol. *Appl Catal Gen*. 2000;196(1):143-155. doi:10.1016/s0926-860x(99)00453-6
28. Sifontes Herrera VA, Saleem F, Kusema B, Eränen K, Salmi T. Hydrogenation of l-arabinose and d-galactose mixtures over a heterogeneous Ru/C catalyst. *Top Catal*. 2012;55(7–10):550-555. doi:10.1007/s11244-012-9833-z
29. Sifontes VA, Rivero D, Wärnå JP, Mikkola J-P, Salmi TO. Sugar hydrogenation over supported Ru/C—kinetics and physical properties. *Top Catal*. 2010;53(15):1278-1281. doi:10.1007/s11244-010-9582-9
30. Najarnezhadmashhadi A, Wärnå J, Eränen K, Trajano HL, Murzin D, Salmi T. Modelling of kinetics, mass transfer and flow pattern on open foam structures in tubular reactors: hydrogenation of arabinose and galactose on ruthenium catalyst. *Chem Eng Sci*. 2021;233:116385. doi:10.1016/j.ces.2020.116385
31. Araujo-Barahona G, Eränen K, Oña JP, Murzin D, García-Serna J, Salmi T. Solid foam Ru/C catalysts for sugar hydrogenation to sugar alcohols—preparation, characterization, activity, and selectivity. *Ind Eng Chem Res*. 2022;61(7):2734-2747. doi:10.1021/acs.iecr.1c04501

32. Zapico RR, Marín P, Díez FV, Ordóñez S. Liquid hold-up and gas–liquid mass transfer in an alumina open-cell foam. *Chem Eng Sci*. 2016;143:297-304. doi:10.1016/j.ces.2016.01.008
33. Turek F, Lange R. Mass transfer in trickle-bed reactors at low Reynolds number. *Chem Eng Sci*. 1981;36(3):569-579. doi:10.1016/0009-2509(81)80145-5
34. Goto S, Smith JM. Trickle-bed reactor performance. Part I. Holdup and mass transfer effects. *AIChE J*. 1975;21(4):706-713. doi:10.1002/aic.690210410
35. Zalucky J, Wagner M, Schubert M, Lange R, Hampel U. Hydrodynamics of descending gas-liquid flows in solid foams: liquid holdup, multiphase pressure drop and radial dispersion. *Chem Eng Sci*. 2017;168:480-494. doi:10.1016/j.ces.2017.05.011
36. Cognet P, Berlan J, Lacoste G, Fabre P-L, Jud J-M. Application of metallic foams in an electrochemical pulsed flow reactor Part I: Mass transfer performance. *J Appl Electrochem*. 1995;25(12):1105-1112. doi:10.1007/BF00242537
37. Lali F. Characterization of foam catalysts as packing for tubular reactors. *Chem Eng Process Process Intensif*. 2016;105:1-9. doi:10.1016/j.cep.2016.04.001
38. Plessis PD. Pore scale modelling for flow through different types of porous environment. In: Delgado J, ed. *Heat and Mass Transfer in Porous Media*. Elsevier; 1992:249-262.
39. Edouard D, Lacroix M, Huu CP, Luck F. Pressure drop modeling on SOLID foam: state-of-the art correlation. *Chem Eng J*. 2008;144(2):299-311. doi:10.1016/j.cej.2008.06.007
40. Giani L, Groppi G, Tronconi E. Mass-transfer characterization of metallic foams as supports for structured catalysts. *Ind Eng Chem Res*. 2005;44(14):4993-5002. doi:10.1021/ie0490886
41. Saber M, Huu TT, Pham-Huu C, Edouard D. Residence time distribution, axial liquid dispersion and dynamic–static liquid mass transfer in trickle flow reactor containing β-SiC open-cell foams. *Chem Eng J*. 2012;185-186:294-299.
42. Hochman JM, Effron E. Two-phase cocurrent downflow in packed beds. *Ind Eng Chem Fundamen*. 1969;8(1):63-71. doi:10.1021/i160029a011
43. Truong Huu T, PhilippeR NP, Edouard D, Schweich D. Radial dispersion in liquid upflow through solid SiC foams. *Ind Eng Chem Res*. 2011;50(8):4329-4334. doi:10.1021/ie1017942
44. Ambrosio G, Bianco N, Chiu WKS, Iasiello M, Naso V, Oliviero M. The effect of open-cell metal foams strut shape on convection heat transfer and pressure drop. *Appl Therm Eng*. 2016;103:333-343. doi:10.1016/j.applthermaleng.2016.04.085
45. Mederos FS, Ancheyta J, Chen J. Review on criteria to ensure ideal behaviors in trickle-bed reactors. *Appl Catal Gen*. 2009;355(1):1-19. doi:10.1016/j.apcata.2008.11.018
46. Schwidder S, Schnitzlein K. A new model for the design and analysis of trickle bed reactors. *Chem Eng J*. 2012;207-208:758-765. doi:10.1016/j.cej.2012.07.054
47. Iordanis A. *Mathematical Modelling of Catalytic Fixed Bed Reactors*. University of Twente; 2002.
48. Metaxas KC, Papayannakos NG. Kinetics and mass transfer of benzene hydrogenation in a trickle-bed reactor. *Ind Eng Chem Res*. 2006;45(21):7110-7119. doi:10.1021/ie060577a
49. Salmi TO, Mikkola J-P, Warna JP, Francis T. *Chemical Reaction Engineering and Reactor Technology*. CRC Press, An Imprint of Taylor And Francis; 2010.
50. Stemmet CP, Bartelds F, van der Schaaf J, Kuster BFM, Schouten JC. Influence of liquid viscosity and surface tension on the gas–liquid mass transfer coefficient for solid foam packings in co-current two-phase flow. *Chem Eng Res Des*. 2008;86(10):1094-1106. doi:10.1016/j.cherd.2008.04.007

SUPPORTING INFORMATION

Additional supporting information may be found in the online version of the article at the publisher's website.

How to cite this article: Najarnezhadmashhadi A, Braz CG, Russo V, Eränen K, Matos HA, Salmi T. Modeling of three-phase continuously operating open-cell foam catalyst packings: Sugar hydrogenation to sugar alcohols. *AIChE J*. 2022;68(9):e17732. doi:10.1002/aic.17732